# Recent Developments of a Coupled CFD/CSD Methodology

Joseph D. Baum[1], Hong Luo[1], Eric L. Mestreau[1], Dmitri Sharov[1], Rainald Löhner[2], Daniele Pelessone[3], and Charles Charman[4]

[1] Center for Applied Computational Sciences, SAIC, McLean, VA 22102, USA
{baum, luo, mestreau, sharov}@apo.saic.com
[2] CSI, George Mason University, Fairfax, VA 22030, USA
lohner@rossini.gmu.edu
[3] Engineering and Software System Solutions, Solana Beach, CA 92075, USA
[4] General Atomics, San Diego, CA 92121,USA

**Abstract.** A recently developed loose-coupling algorithm that combines state-of-the-art Computational Fluid Dynamics (CFD) and Computational Structural Dynamics (CSD) methodologies has been applied to the simulations of weapon-structure interactions. The coupled methodology enables cost-effective simulation of fluid-structure interactions with a particular emphasis on detonation and shock interaction. The coupling incorporates two codes representing the state-of-the-art in their respective areas: FEFLO98 for the Computational Fluid Dynamics and DYNA3D for the Computational Structural Dynamics simulation. An application of the methodology to a case of weapon detonation and fragmentation is presented, as well as fragment and airblast interaction with a steel wall. Finally, we present results of simulating airblast interaction with a reinforced concrete wall, in which concrete and steel rebar failure and concrete break-up to thousands of chunks and dust particles are demonstrated.

## 1 Introduction

Several classes of important engineering problems require the concurrent application of CFD and CSD techniques. Among these are: a) Shock/structure interactions; b) Aeroelasticity of flexible thin flight structures; c) Hypersonic flight vehicles (thermal-induced deformations); d) Deformation of highly flexible fabrics; and e) Vehicles with variable geometry. Currently, these problems are solved either iteratively, requiring several cycles of "CFD run followed by CSD run", or by assuming that the CFD and CSD solutions can be decoupled.

The various efforts to develop a fluid/structure coupling can be classified according to the complexity level of the approximations used for each of the

V.N. Alexandrov et al. (Eds.): ICCS 2001, LNCS 2073, pp. 1087–1097, 2001.

domains. Approximations of the Partial Differential Equations for the structural mechanics range from simple 6 DOF integration to finite elements with complex models for elasto-plastic materials with rupture laws and contact. Similarly, the fluid dynamics approximations of the PDEs range from the potential flow (irotational, inviscid, isentropic flows) to the full Navier-Stokes set of equations. Our present research interests focus on non-linear applications, in particular, structures that experience severe deformations due to blast loads, aerodynamic or aero-thermodynamic loads. The fluid approximation chosen is either Euler or Reynolds-Averaged Navier-Stokes. On the structure side, elasto-plastic materials with rupture criteria are used.

In this study, the coupled CFD/CSD methodology is applied to the simulation of weapon detonation and fragmentation. This application constitutes a very severe test to the numerical methodology as it requires modeling of several complex, interacting physical phenomena: a) Detonation wave initiation and propagation; b) CSD modeling of case expansion and fragmentation; c) The transfer of rigid fragments from the CSD to the CFD modules; d) Blast wave expansion through the breaking case, diffracting about the flying fragments; e) Flight of thousands of rigid bodies, each treated as a separate, free-flying body, where its trajectory and velocity are determined by balance of forces and moments; and f) Fragments and airblast impact on the structure and the resulting structural deformation.

Two approaches can be used to tackle fluid/structure interaction. The so-called 'tight coupling' approach requires solving both CFD & CSD as one coupled set of equations, and would require the complete rewrite of both solvers. The second approach, termed 'loose coupling', decouples the CFD and CSD sets of equations and uses projection methods to transfer interface information between the CFD and CSD domains. We adopted the latter method. By building on pre-existing and well- established codes, a loose-coupled solver can be assembled with minimum modifications to either of the two solvers. The modularity is kept by the addition of a 'controller' code, which handles the transfer of information between the different solvers [7], [11], [3]. This code handles non-matching meshes at the interface and incorporates conservative interpolation schemes and fast techniques for neighbor search. It deduces automatically the correspondence between fluid and structure points without any user input. Time synchronization between the CFD and CSD solvers is also managed by the controller code, which uses a leap-frog approach.

### 1.1 The Current Numerical Methodology

Mesh generation was performed using FRGEN3D, an advancing front based grid generator [9]. This mesh generator is also included in the flow solver, FEFLO98, to handle mesh regeneration on the fly. The mesher requires the input of CAD surfaces and lines. Very complex shapes can now be meshed in a matter of hours once the model is properly defined [1], [2], [3]. However, assembling the CAD definition of the model still remains the bottleneck, consuming large amounts of man-hours. To remedy this deficiency, we have developed a dedicated graphic

pre-processor, to promptly handle the specifics of the mesher/solver such as: boundary conditions, element size definition and automatic generation of the structural model from the predefined fluid domain. The pre-processor also provides extensive data checking allowing a considerable gain in productivity. For the current study, both CFD & CSD meshes were generated with FRGEN3D. The CFD mesh is composed of tetrahedral elements in the volume and triangles on the surfaces. The CSD mesh includes beams, quad and triangle shells (quads corresponds to the concatenation of 2 triangles) and bricks for the volume. The bricks result from the cut of tetrahedral elements. Although the angles of a typical hex are less than perfect, extensive testing against perfect-angle bricks for both linear and nonlinear tests, produced almost identical results. This, nevertheless, necessitated the replacement of the Belytschko-Tsay hourglass control model (default model in DYNA3D [15]), with the Flanagan-Belytschko hourglass control model (model no. 3 in DYNA3D [5]), incurring a 30% performance penalty.

The flow solver is FEFLO98, a 3-D adaptive, unstructured, edge-based hydrosolver based on the Finite-Element Method Flux-Corrected Transport (FEM-FCT) concept [8]. It solves the Arbitrary Lagrangean-Eulerian (ALE) formulation of the Euler and Reynolds-Averaged turbulent, Navier-Stokes equations. The high order scheme used is the consistent-mass Taylor-Galerkin algorithm. Combined with a modified second-order Lapidus artificial viscosity scheme, the resulting scheme is second-order accurate in space, and fourth-order accurate in phase. The spatial adaptation is based on local H-rfinement, where the refinement/deletion criterion is a modified H2-seminorm [10] based on a user- defined unknown. For detonations and shock wave diffraction simulations, the critical parameter used for the refinement/deletion criteria is density. The explosive detonation is modeled using a JWL equation of state with afterburning. To enhance computational efficiency, the portion of the fluid domain not reached by the blast wave is automatically deactivated.

The structural dynamics solver is DYNA3D [15], an unstructured, explicit finite element code. DYNA3D is well suited for modeling large deformations and provides a good base for non-linear materials with elasto-plastic compartmental laws with rupture. DYNA3D incorporates a large library of materials and various equations-of-state, as well as many kinematic options, such as slidelines and contacts. Furthermore, DYNA3D is a well proven and benchmarked solver used extensively in the CSD community.

## 2 Numerical Results

### 2.1 Weapon Fragmentation Study

The coupled technology has been applied to the simulation of the detonation and fragmentation of an experimental weapon. The bomb hangs tip-down at the center in a reinforced concrete room The thick- walled steel weapon is top (i.e., base) ignited. The detonation front propagates from the base to the tip at the C-J detonation velocity, as prescribed in the detonation model (essentially, the

program burn model of DYNA3D). Initially, the CFD domain consisted of two separate regions: the domain inside the case is modeled using the JWL EOS, while the ambient atmosphere outside is modeled using a perfect gas EOS. Once fragmentation occurred, the two topologies merged and the complete domain is modeled using the JWL EOS.

The structural response (case expansion) is modeled using GA-DYNA [12], [13], the General Atomics version of DYNA3D. Several CSD meshes of this weapon were tested, using either 8-node hexahedral elements or brick-like parallelepipedal elements, and varying the number of elements from 748 to 8228. The results presented here were obtained with 748 brick elements with a single element across the thickness of the casing. The fragment size distribution for the present simulation **is prescribed**. This value was obtained by averaging fragment sizes from several arena tests. A more accurate procedure is described below [14].

After ignition, as the detonation wave propagates from the base to the tip, the high-pressure detonation products force the case to expand. The structural elements fail once the element strain (averaged over all faces) exceeds 100%. The strain criterion for failure is computed at the center of each element. Each failing fragments is then treated as a separate rigid body, for which the trajectory is computed using a 6 DOF integrator linked to the contact algorithms. Once bricks fail, fluid elements are introduced into the narrow gaps separating the fragments. The gaps are of the order of a millimeter, which would result in unacceptable small fluid elements and small integration time step. The gap size was increased by shrinking the fragments uniformly around the center of gravity. The topology change due to the breakup requires remeshing of at least part of the domain, a CPU intensive process that is allowed to occur only every 5-8 $\mu$s. Thus, the CSD code maintains a list of failed elements, and shrinks them only when allowed.

One important aspect of this class of simulations is the large size disparity between the critical length scales. After fragment break-up, the gap between fragments is several **millimeters**. In contrast, the average fragment length is about ten **centimeters**, and the room length is of the order of ten **meters**. The large disparity in dimensions forced us to attach to each flying fragment entities called grid sources. The sources enforce local pre-specified element size, ensuring a uniform, high-resolution mesh about each fragment, and thereby reduce the number of local and global remeshings. Figures 1a through 1c show the CSD surface mesh, the CFD mesh on a planar cut through the weapon (not a plane of symmetry due to the lack of symmetry for this weapon), and the CFD surface mesh, respectively, at 550 $\mu$s. The results show the finely-resolved mesh within the initial HE zone, resulting from the application of a grid source placed along the center of the weapon. On the weapon we form a much finer CFD mesh than the CSD mesh, with rapid increase of mesh size with distance from the weapon. The range-of-influence of the centerline-placed source was specified to produce a fine-resolution mesh not just within the HE zone, but also around the complete volume in which fragmentation occurs after case expansion. As the fragments exit the fine-resolution zone imposed by the central source, CFD mesh resolution

is reduced to the level specified by the sources attached to the fragment. This can clearly be seen on the third row from the top, where mesh resolution is reduced from several elements across each fragment at t=0, to three elements at t=350 $\mu$s, and finally two elements at t=550 $\mu$s (Fig 1c). Finally, examination of the planar cut results (Fig 1b) shows that the mesh size dictated by the sources is dependent on the fragment and face size. Sources attached to the smaller moving faces yield a finer mesh resolution than those attached to the larger ones. Thus, at t=550 $\mu$s, the large fragments that are outside the core central source (such as the rows 4, 15 and 17), show coarse mesh resolution on the large faces, but fine resolution within the gaps and the near-by faces.

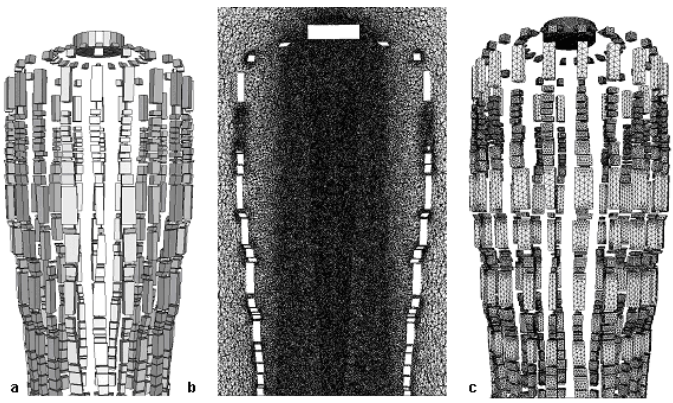


**Fig. 1.** CSD mesh, CFD mesh on a plane cut and CFD mesh on the surface of the weapon at t=0.550ms

During case expansion, the internal mesh velocity significantly exceeds the external velocity, resulting in case thinning. On average, while the CG of the element experiences a 100% strain (break-up criteria), the internal face expands about 145-160%, compared to about 70-80% for the external face. This indicates that during a significant portion of the expansion period, the internal face velocity is about twice the external face velocity.

Figures 2a through 2d show a sequence of snapshots. At each time, the panel shows the pressure and CFD mesh velocity contours on a planar cut through the weapon, and the CSD fragment velocity contours. Figure 2a at 131 $\mu$s shows detonation wave propagation down (from base to tip) as a planar front, and the radial expansion of the case. The first fragment break-up occurs at 94 $\mu$s, for the upper row attached to the heavy base. While the base itself does not fragment, as it does not expand significantly, the row of elements below fails due to shear, not tension. Similarly, the layer of fragments above the nose cone fails due to shear (Fig 2c at 370 $\mu$s). Detonation was completed at about t=263 $\mu$s and the shock reflected upward (Fig 2b).

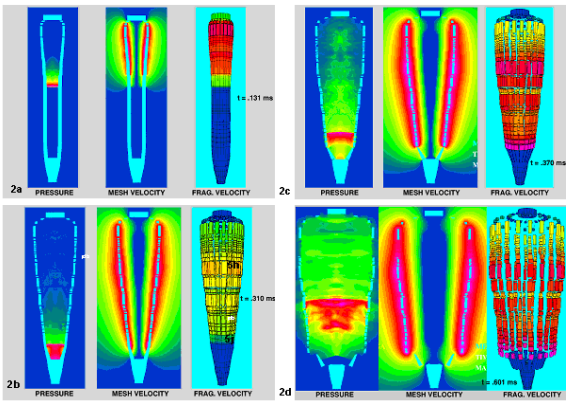


**Fig. 2.** Propagation of detonation wave and case fragmentation. Results show pressure, mesh velocity, and fragment velocity at times 131 $\mu$s, 370 $\mu$s, and 600 $\mu$s, respectively.

The relatively small spacing between the expanding fragments ensures that the high-pressure detonation products would be fairly contained within the expanding fragments for an extended period. The results demonstrate that even at t=0.6 ms (Fig 2d), the pressure within the core is significantly higher than outside.

The fragments achieve their terminal velocity within about 120-150 $\mu$s after detonation front passage. This is significantly slower then the acceleration period of 60-90 $\mu$s for a serrated weapon [4]. The final mass-averaged fragment velocity obtained for this simulation, using a strain break-up value of 1.0, was 787.6 m/sec. The experimental measured value was 752 m/sec. To examine the role of the break-up strain value on the final velocity we conducted three more simulations, at break-up strain values of 0.1 ($V_f$=675.53 m/sec), 0.5 ($V_f$=741.8 m/sec), and infinity (no break-up, $V_f$=859.7 m/sec). The results show that the experimental data indicates a break-up strain value of about 0.6, a value that corresponds to an internal expansion of about 90%, and external expansion of about 50%.

A total of five simulations were conducted under this study, investigating the role of the break-up strain value on the final fragmentation velocity distribution, and single vs. multiple elements through the case thickness. The initial mesh for each simulation included about 8.7 million elements, the final one about 19.2 million elements. The five simulations conducted averaged about five days on a SGI Origin 2000, using twelve to sixteen processors. Once remeshing parallelization was completed, CPU time was cut to less than a day.

### 2.2 Blast Impact on a Reinforced Concrete Wall

As the next step in the CFD/CSD coupling development effort, we applied the coupled methodology to the simulation of airblast interaction with reinforced

concrete wall. The model included two rooms, but only the connecting wall was modeled with the CSD code. All other structural components (e.g., other walls, floor and ceiling) were treated as rigid. The CFD domain consisted of 9,387 boundary points, 55,281 points and 296,751 elements. The wall included 81,101 nodes, 69,048 solid hexahedron elements in the concrete and 598 beam points in the steel rebars. While the CFD solution was non- adapted, three levels of mesh adaptation [12] were in the CSD model. The standard DYNA3D element erosion model was used to eliminate failed CSD elements.

Several new schemes were employed here. These include: 1) A recently developed crack propagation model [14] that takes advantage of the CSD H-refinement scheme. As the crack propagates through the material, mesh adaptation is used to ensure the accuracy of the stress wave propagation, and the accurate agglomeration of the elements into discrete fragments. This approach alleviates the need for expensive arena test data. The new model was validated against data for two test [14]; 2) The adaptation procedure ensures that each fragment contains several elements. As the elements fail and fragments are formed, each is treated by GA-DYNA as an independent body, with the appropriate volume, mass, momentum and energy. GA-DYNA then keeps track of fragment-to-fragment and fragment-to-wall interactions through a contact algorithm. GA-DYNA transfers the information to FEFLO98, which treats every fragment as a sphere, allowing for accurate momentum and energy exchange (e.g., drag and heat transfer); and 3) A new model that allows rebar data to be interpolated from enclosing elements, in contrast to the original DYNA3D that required all nodes to be on the rebar itself.

Figure 3 shows several snapshots taken during the simulation. Fig. 3a shows the CSD mesh as shown on the surface. Notice that the CSD elements were generated by splitting the CFD elements (as clearly seen on the sides). The steel rebars are shown in Fig 3b. The concrete material used was intentionally 'softened' to produce faster wall break-up (for testing and debugging purposes). Hence, the significant damage shown in Fig. 3c, after only 400 time steps. Each element face is given a uniform color corresponding to the value of the element damage parameter. No nodal averaging was performed. Figures 3d, 3e and Figs 3d, 3g show a pair of snapshots (front and back) taken early and late in the run, respectively. The figures show the computed geometry as realized by the CSD code (Figs 3d and 3f), and as realized by the CFD code (Figs 3e and 3g). While the CSD code integrates all structural matter, including all the produced debris, small particles and dust, not all information is transferred to the CFD code. Only information about large chunks and large fragments is transferred to the CFD code. These are treated by the CFD code as moving bodies. Thus, the CFD code computes the motion of hundreds of moving bodies, evaluating the forces acting on them and the resulting trajectories. Small particles and dust trajectories are carried by the CSD code, and only the momentum and energy transfer information is exchanged with the CFD code, so that the CFD code can accurately compute energy dissipation due the drag and thermal losses imposed by the flying smaller, cooler particles. Figures 3h and 3i show a superposition of

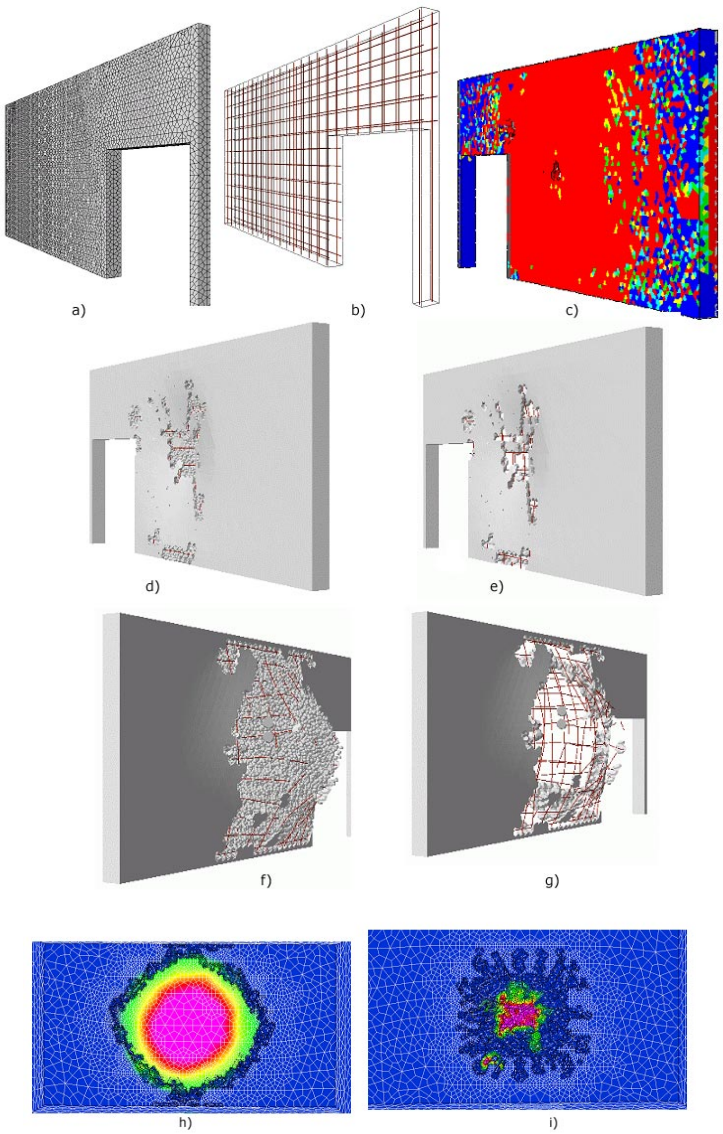


**Fig. 3.** This figure shows the initial CSD mesh, and the structural response to blast. The figures show the CSD surface mesh (Fig 3a); the rebar pattern (Fig 3b); the element damage parameter after 400 steps (Fig 3c); the CSD and CFD surface realizations at early time (Figs 3d and 3e), and late time (Figs 3f and 3g), respectively; a superimposed pressure contours and adapted CSD mesh at an early time on the front and back faces of the damaged wall (Figs 3h and 3i, respectively).

pressure contours and CSD mesh on both sides of the wall. The results show the typical damaged concrete pattern: a crown in the blast room and spallation web on the opposite side. Notice the complex connectivity through the concrete that allows the high pressure to emerge through the other side of the wall: from the peripheral crown to the centered spall zone. Three levels of mesh adaptation are shown in these figures. The adapted CSD mesh enables accurate prediction of the spallation, crack propagation, element failure and fragment formation, which expose the rebars on the spalled side.

### 2.3 Blast Fragment Impact on a Steel Chamber

The coupled CFD/CSD methodology was applied to the simulation of airblast and fragment interaction with a steel walled chamber. While the CFD solution was non-adapted, three levels of mesh adaptation [Pe97] were in the CSD model. The standard DYNA3D element erosion model was used to eliminate failed CSD elements.

The numerical predictions show that the impacting weapon fragments arrive ahead of the airblast (Fig 4a), punching holes through the plate (Figs 4b, 4c and 4e). Next, the pressure blast from the detonation tears the weakened plate apart (Figs 4d and 4f). The eroded plate elements were converted into particles that can interact with the rest of the structure. Contact conditions were enforced between all entities of the model, thus avoiding simulation break due to fragments coming in contact with each other and eliminating the CFD mesh in between.

Significant CPU cost reduction was achieved by the allowing the CSD code to model convection of the small broken pieces. The CFD code handles these pieces as spheres with the correct effective radius, modeling only the momentum (drag) and energy exchange between the blast and the spheres. Hence, the information transferred from the CSD to the CSD module is reduced to the minimal sphere data (radius, density, velocity vector and temperature).

## 3 Summary and Conclusions

A recently developed loose-coupling algorithm that combines state-of-the-art Computational Fluid Dynamics (CFD) and Computational Structural Dynamics (CSD) methodologies, has been applied to the simulation of weapon detonation and fragmentation. This application required modeling several complex and interacting physical phenomena. In addition to the loose coupling of two state-of-the-art codes, FEFLO98 and DYNA3D, several new routines were developed to allow better communications between the codes, especially during case fragmentation. The results demonstrate the ability of the coupled methodology to handle these processes and yield results that are in good agreement with experimental data. While other techniques may be used to model weapon fragmentation, the advantage of the coupled CFD/CSD methodology is that in addition to the fragment size and velocity distribution, it also yields an accurate description of the airblast environment. The resulting fragment and airblast predictions can then be used to predict the target response to the attack.

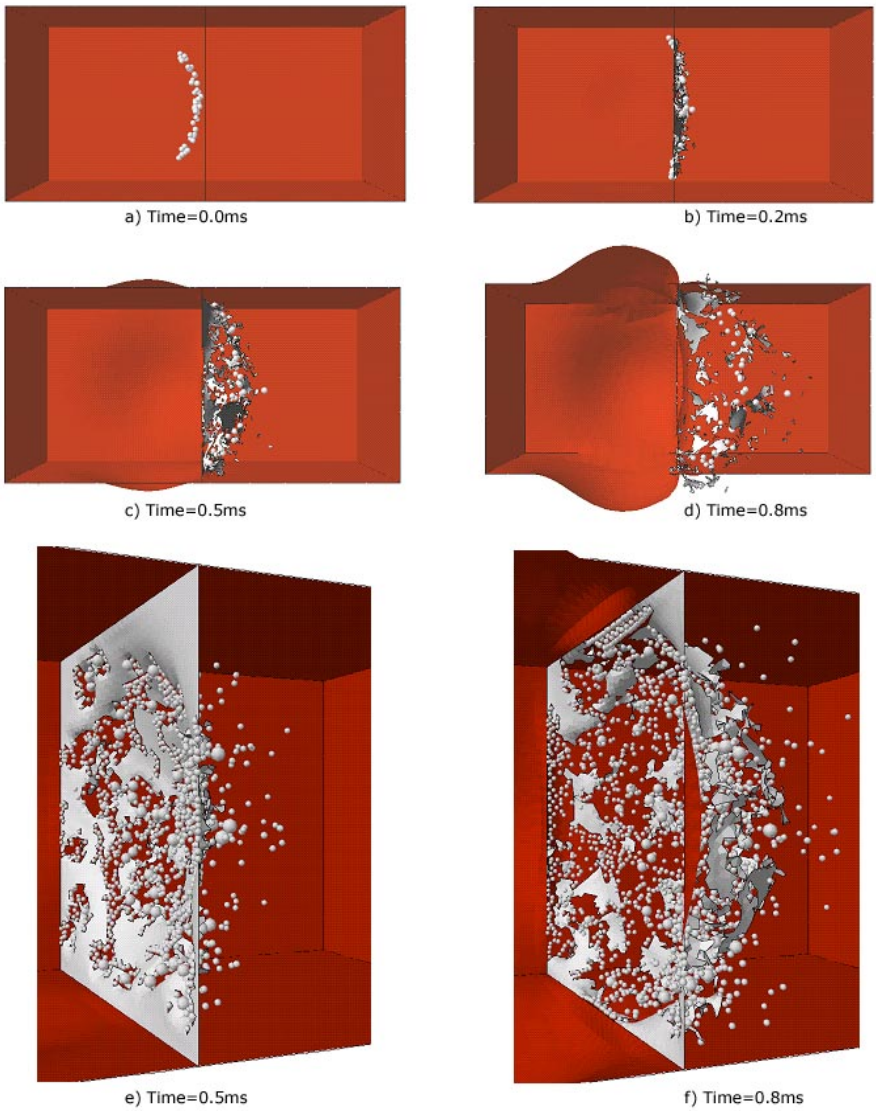


**Fig. 4.** Figures 4a shows the initial fragment position; Fig. 4b shows the surface immediately after fragment impact (t=0.2 ms); Figs 4c and 4e show the steel surface at t=0.5ms, after fragment impact but before airblast impact, while Figs 4d and 4f show the complete repture of the steel plate after blast impact.

## 4 Acknowledgements

This research effort was supported by the Defense Threat Reduction Agency. Dr. Michael E. Giltrud, served as the contract technical monitors. Computer time was generously provided by the DOD High Performance Computing Modernization Office (HPCMO).

## References

1. J.D. Baum, H. Luo, and R. Löhner : Numerical Simulation of a Blast Inside a Boeing 747; AIAA-93-3091 (1993).
2. J.D. Baum, H. Luo and R. Löhner : Numerical Simulation of Blast in the World Trade Center; AIAA-95-0085 (1995).
3. J.D. Baum, H. Luo, R. Löhner, C. Yang, D. Pelessone and C. Charman : A Coupled Fluid/Structure Modeling of Shock Interaction with a Truck; AIAA-96-0795 (1996).
4. J.D. Baum, H. Luo and R. Löhner : The Numerical Simulation of Strongly Unsteady Flows With Hundreds of Moving Bodies; AIAA-98-0788 (1998).
5. T. Belytschko, and J.I. Lin : A Three-Dimensional Impact-Penetration Algorithm with Erosion; Computers and Structures, Vol. 25 No. 1, p 95, 1986.
6. D.J., Benson, and J.O. Hallquist : A single surface contact algorithm for the post-buckling analysis of shell structures; Computational Methods in Applied Mechanics and Engineering, Vol. 78, No. 2 p 141, 1990.
7. J.R. Cebral and R. Löhner : Conservative Load Transfer for Fluid-Structure-Thermal Simulations; Proc. 4th WCCM, Buenos Aires, Argentina, July (1998).
8. R. Löhner, K. Morgan, J. Peraire and M. Vahdati : Finite Element Flux-Corrected Transport (FEM-FCT) for the Euler and Navier-Stokes Equations; Int. J. Num. Meth. Fluids 7, 1093-1109 (1987).
9. R. Löhner and P. Parikh : Three-Dimensional Grid Generation by the Advancing Front Method; Int. J. Num. Meth. Fluids 8. 1135-1149(1988).
10. R. Löhner and J.D. Baum : Adaptive H-Refinement on 3-D Unstructured Grids for Transient Problems; Int. J. Num. Meth. Fluids 14, 1407-1419 (1992).
11. R. Löhner, C. Yang, J. Cebral, J.D. Baum, H. Luo, D. Pelessone and C. Charman : Fluid- Structure Interaction Using a Loose Coupling Algorithm and Adaptive Unstructured Grids; AIAA-95-2259 (1995).
12. D. Pelessone, and C.M. Charman : An Adaptive Finite Element Procedure for Structural Analysis of Solids; 1997 ASME Pressure Vessels and Piping Conference, Orlando, Florida, July (1997).
13. D. Pelessone and C.M. Charman : A General Formulation of a Contact Algorithm with Node/Face and Edge/Edge Contacts; 1998 ASME Pressure Vessels and Piping Conference, San Diego, Ca, July (1998).
14. D. Pelessone, C.M. Charman, R. Löhner and J.D. Baum : A new Crack Propagation Algorithm for modeling Weapon Fragmentation; in preparation.
15. R.G. Whirley and J.O. Hallquist : DYNA3D, A Nonlinear Explicit, Three-Dimensional Finite Element Code for Solid and Structural Mechanics - User Manual; UCRL-MA-107254 (1991), also Comp. Meth. Appl. Mech. Eng. 33, 725-757 (1982).